2020

Debris flow enlargement from entrainment: A case study for comparison of three entrainment models

Ping Shen
Hong Kong University of Science and Technology

Limin Zhang
Hong Kong University of Science and Technology

Ho Fai Wong
Technological and Higher Education Institute of Hong Kong, ceshfw@vtc.edu.hk

Dalei Peng
Technological and Higher Education Institute of Hong Kong

Shengyang Zhou
Hong Kong University of Science and Technology

See next page for additional authors

Recommended Citation

Shen, P.,Zhang, L.,Wong, H.,Peng, D.,Zhou, S.,Zhang, S.,& Chen, C. (2020). Debris flow enlargement from entrainment: A case study for comparison of three entrainment models. *Engineering Geology, 270*. http://dx.doi.org/10.1016/j.enggeo.2020.105581

Engineering Geology 270 (2020) 105581

Contents lists available at ScienceDirect

Engineering Geology

journal homepage: www.elsevier.com/locate/enggeo

Debris flow enlargement from entrainment: A case study for comparison of three entrainment models

Ping Shen[a], Limin Zhang[a,*], Ho Fai Wong[b], Dalei Peng[b], Shengyang Zhou[a], Shuai Zhang[c], Chen Chen[d]

[a] Department of Civil and Environmental Engineering, The Hong Kong University of Science and Technology, Clear Water Bay, Hong Kong
[b] Technological and Higher Education Institute of Hong Kong, Tsing Yi Island, New Territories, Hong Kong
[c] MOE Key Laboratory of Soft Soils and Geoenvironmental Engineering, Zhejiang University, Zheda Road #38, Hangzhou 310027, China
[d] State Key Laboratory of Hydraulics and Mountain River Engineering, College of Water Resource and Hydropower, Sichuan University, No. 24 South Section 1, Yihuan Road, Chengdu 610065, Sichuan, China

ARTICLE INFO

Keywords:
Landslide
Landslide risk
Debris flow
Entrainment
Numerical simulation

ABSTRACT

Material entrainment can significantly magnify debris flow volume and increase its destructive power. Despite great research efforts, entrainment is still not well understood. To meet the needs for debris flow simulation and hazard analysis, it is of practical significance to understand and evaluate existing entrainment models. In this study, we evaluate three entrainment models on an integrated single-phase continuum debris flow simulation platform. The well-documented Tsing Shan debris flow in 1990 in Hong Kong, with an initial landslide volume of 2500 m^3 and a final deposit volume of 20,400 m^3, is used as a benchmark to compare the three models. The characteristics and performance of each model and its model parameters are discussed. Although numerical results achieve reasonable agreement with detailed field investigations, some parameters are still determined empirically and subjectively. Despite of the imperfection, these models can be used for debris flow hazard analysis in the Hong Kong region with similar conditions. More physically-based entrainment models considering two-phase flow need to be adopted and further developed in the future.

1. Introduction

Debris flow often occurs in mountainous areas amidst heavy rainfall, for example in Hong Kong. It could be very disastrous, swallowing and destroying nearly everything on its marching path and causing intolerable threats to unprotected people's lives, properties and infrastructures (Mergili et al., 2017, 2018a). Debris flow can carry a large amount of solid materials (mainly soil and rock, often with some wood debris) off slopes and channels through entrainment or erosion; the magnitude of the final debris flow volume could be many times of its initial volume (Iverson et al., 2011; Pudasaini and Fischer, 2016). The destructive power of a debris flow can be grossly underestimated if the entrainment of material is ignored. Therefore, studying the entrainment process is crucial to debris flow hazard analysis and risk assessment.

Material entrainment is a complex process. Entrainment mechanisms include bed erosion and instability of stream banks undercut by bed erosion (Hungr et al., 2005). The erosion of bed material is a result of drag, shear and other forces acting at the base of the flow, aided by the loss of shear strength due to rapid undrained loading (Hutchinson and Bhandari, 1971), impact loading, or liquefaction of the saturated channel fills (Sassa and Wang, 2005). There are many volume-magnifying debris flow events in mountainous areas. In Hong Kong, the Tsing Shan area experienced a typical volume-magnifying debris flow in 1990 (Fig. 1). The initial landslides of about 2500 m^3 evolved into a large debris flow of about 20,400 m^3. King (2013) conducted comprehensive field investigations and laboratory tests on this debris flow. Similar debris flow enlargement events also occurred worldwide, as shown in Table 1. The enlargement of debris flow volume plays a very important role in determining the final magnitude of debris flows (Pudasaini and Fischer, 2016).

Great efforts have been made to develop numerical models for simulating debris flow mobility (e.g. O'Brien et al., 1993; Hungr and McDougall, 2009; Pastor et al., 2009; Quan Luna et al., 2012; Pudasaini, 2012; Dai et al., 2014; van Asch et al., 2014; Chen and Zhang, 2015; Chen et al., 2017; Mergili et al., 2018a,b; Shen et al., 2017, 2018; Li et al., 2018, 2019; Zhou et al., 2019), as well as to

* Corresponding author.
E-mail addresses: pshen@connect.ust.hk (P. Shen), cezhangl@ust.hk (L. Zhang), pdchbsz@vtc.edu.hk (D. Peng), szhouaq@connect.ust.hk (S. Zhou), zhangshuaiqj@zju.edu.cn (S. Zhang), laurachen@scu.edu.cn (C. Chen).

https://doi.org/10.1016/j.enggeo.2020.105581
Received 13 September 2019; Received in revised form 4 March 2020; Accepted 5 March 2020
Available online 06 March 2020
0013-7952/

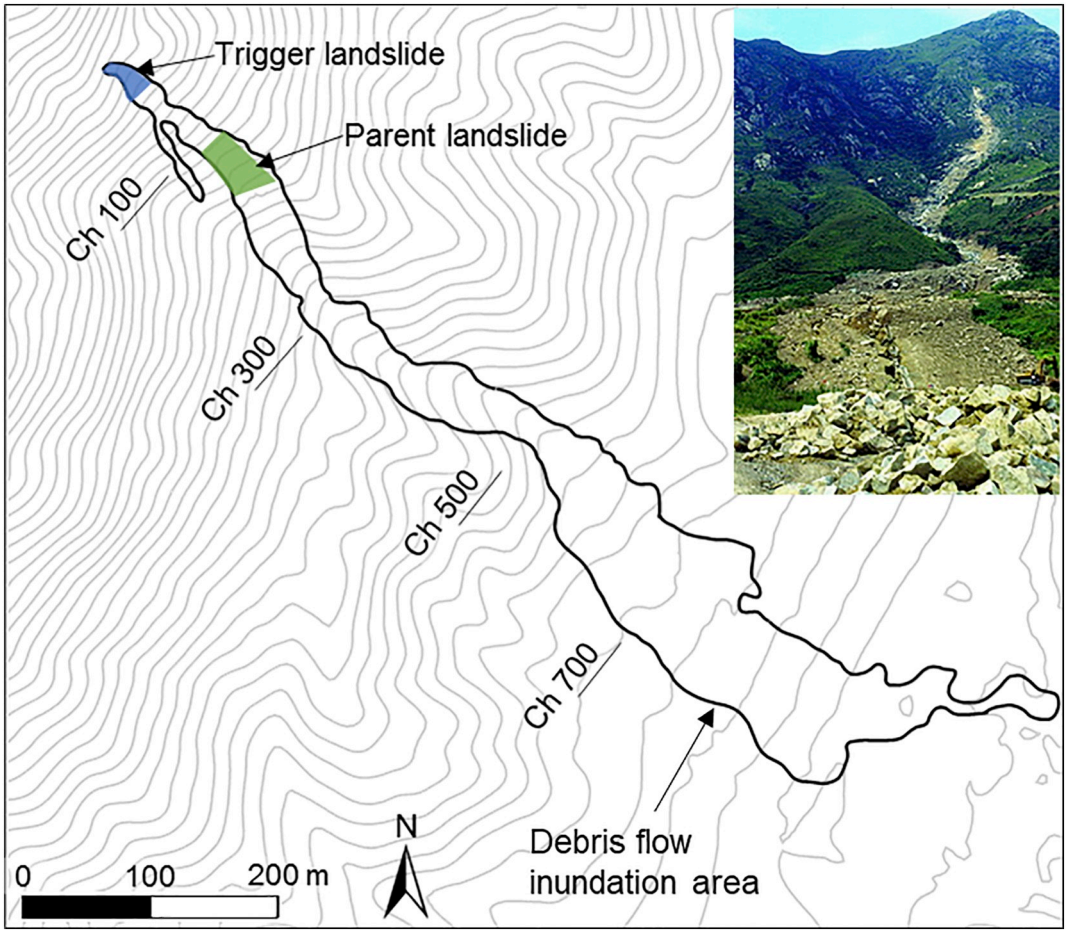

Fig. 1. The 10 m contours of the 1990 Tsing Shan debris flow site. A landslide of about 350 m^3 initiated the debris flow. The curved area indicates the flow inundation area. The detached ground mass dashed down the hill for about 100 m and triggered a larger landslide of about 2000 m^3, which subsequently developed into a debris flow of about 20,000 m^3 through entrainment of bed colluvium materials along its runout path. (Insert photo, courtesy of Hong Kong Slope Safety Website: http://hkss.cedd.gov.hk/hkss/eng/index.aspx, Geotechnical Engineering Office, Civil Engineering and Development Department).

Table 1
Summary of debris flow enlargement cases.

Date	Location	Initial volume (m^3)	Final volume (m^3)	Amplification factor	Initiation mechanism	Reference
11 Sept. 1990	Tsing Shan, Hong Kong	2500	20,400	8.2	Landslide transformation	King (2013)
12 June 1997	Dolomites, Italy	600	6000	10.0	Erosion	Berti et al. (1999)
11 July 1997	British Columbia, Canada	25,000	92,000	3.7	Landslide transformation	Jakob et al. (2000)
29 June 1999	Hiroshima, Japan	250	5000	20.0	Landslide transformation	Wang et al. (2003)
8 May 2004	Fjærland, Norway	25,000	240,000	9.6	Erosion	Breien et al. (2008)
14 Aug. 2010	Yingxiu, China	183,000	805,000	4.4	Landslide transformation/Erosion	Li et al. (2012)

conduct laboratory and field experiments (e.g. Iverson et al., 2011; Ren et al., 2018; Wang et al., 2018; Yang et al., 2018). Physically-based entrainment models have been embedded in continuum-based numerical models, which are generally depth-integrated and reduced to two-dimensional problems (e.g. Iverson and Ouyang, 2015; Pudasaini and Fischer, 2016; Li et al., 2018). Besides, basal entrainment models have been extensively applied (e.g. McDougall and Hungr, 2005; Medina et al., 2008; Iverson et al., 2011; Iverson, 2012; Quan Luna et al., 2012; Iverson and Ouyang, 2015; Li et al., 2018; Zhang et al., 2019). Particularly, Ouyang et al. (2015) adopted an entrainment rate formula that satisfies a boundary momentum jump condition and combines the Coulomb friction model and the Voellmy friction model to overcome their individual flaws. Pudasaini and Fischer (2016) developed a fully mechanical two-phase erosion model and addressed several long-standing issues including the rigorous proof of erosion-enhanced mobility in mass flows and removing the singularity problem in previously models. Kwan and Sun (2007) proposed a modelling program, 3dDMM (3d Debris Mobility Model), to simulate the runout process of the 1990 Tsing Shan debris flow as a benchmarking exercise for landslide mobility simulation. This model simulates the runout process and deposition area well. The entrainment process in 3dDMM is on a grid basis at every time step and the erosion rate is assumed to be proportional to the grid velocity and debris depth.

Despite the aforementioned great efforts in studying the entrainment mechanisms and developing numerical models, the entrainment process is very complex and not yet well understood. As a result, the simulation of entrainment in debris flows is still very challenging. To meet the needs for debris flow simulation and model selection, it is of practical significance to evaluate and compare practical entrainment analysis models.

The objective of this study is to evaluate three entrainment analysis models for debris flow simulation. The 1990 Tsing Shan debris flow,

which is a typical well-documented debris flow and entrainment case, is used as a benchmark to assess the performance of these entrainment models on an integrated debris flow simulation tool EDDA 2.0 (Shen et al., 2018). In the present study, the entrainment process of the Tsing Shan debris flow is simulated using three entrainment models. The performance of these entrainment models is evaluated and the characteristics of each model are discussed. The results serve as a reference for selecting numerical models for hazard analysis and risk assessment, which further emphasizes the importance of properly simulating debris flow events by employing advanced two-phase mechanical erosion models.

2. The 1990 Tsing Shan debris flow

2.1. Study area

Tsing Shan is located in western New Territories, Hong Kong, about 2 km west of Tuen Mun Valley. The study area includes the whole catchment from the ridgeline at the summit of Tsing Shan to the cut slope and platform in the downstream area (Fig. 1). The summit rises to 583 mPD (meters above Hong Kong Principal Datum) and is the highest peak in the study area. Chan et al. (1991) developed a chainage to indicate the distance from the starting point to anywhere along the debris flow path. “Ch” means the chainage line. For example, “Ch 0” denotes the starting point of the chainage line and “Ch 500” denotes the chainage point 500 m downstream the starting point. The whole debris flow path can be divided into two parts at the mouth of the drainage line (Ch 500): the upper slope area and the lower deposition area. The total relief in altitude in the study area is 310 m, shown in the discrete elevation model (Fig. 2a).

The detailed engineering geological map of this area was created by Geotechnical Engineering Office (GEO) shown in drawings GEO/P/PTE/1 and GEO/P/PTE/2 in GEO Report No. 281 (King, 2013). In this paper, the geological settings of the debris flow area can be broadly classified into three types (Fig. 2b): the fine grained granite in the upper part; the sedimentary rocks containing sandstone, siltstone and mudstone in the middle part; and the volcanic rock in the lower part. The superficial deposits above the bedrock are Pleistocene and Holocene, referred to as colluvium in this study.

The vegetation on the summit and upper slopes is generally only grass. On the side slopes are sparse patches of scrubby bushes and small trees. The distribution becomes denser and the vegetation becomes larger closer to the main valley.

2.2. The debris flow event

A debris flow occurred in the study area in the early morning on 11 Sept. 1990. This debris flow was witnessed by a local resident, who was awaken by the pitter-patter of heavy rainfall, light vibrations and noises, and heard the loud noises of the debris flow later at about 03:00. The noises continued for less than 30 min. Therefore, the debris flow was shown to start sometime before 03:00 and lasted for about half an hour. After the occurrence of the debris flow, the GEO has conducted a comprehensive study of the disaster (King, 2013). Digital elevation data with high resolution of 5 m has been prepared to facilitate numerical simulation of the debris flow. Detailed field investigations and aerial photo interpretation were carried out to deliver thorough information about the geology and geomorphology of the study area. Basic information about soil and debris deposits was also collected, such as particle size distribution. The entrainment and deposition process along the debris flow path was well documented, which provides evidence to validate debris flow entrainment models.

The Tsing Shan debris flow was a complex geomorphological event. The whole process might be divided into four sub-events. Initially, a small “trigger” landslide of about 350 m^3 at the origin of the track was triggered by heavy rainfall. Then another larger “parent” landslide at Ch 100 with a volume of about 2500 m^3 was initiated by the “trigger” mass and intensified the debris flow. After that, the landslide materials formed large pulses of channelized debris flow that eroded and entrained colluvium. Then the channelized debris flow surged down the drainage line, entraining colluvium of about 19,000 m^3. Finally, the debris flow accumulated in the deposition area and the ongoing rainfall continued to cause erosion of the debris deposit beyond the mouth of the drainage line. Inferred from the observed relatively uniform and thin deposit, the main mechanism of debris movement in this event is “flowing” among several possible mechanisms including “rolling, bouncing and sliding”.

Some physical parameters were also interpreted. The maximum erosion depth was in the range of 3–4 m. The flowing velocity was estimated to be 16.5 m/s at Ch 350 and 12.5 m/s at Ch 475 by using the equations from Johnson and Rodine (1984). Finally, the debris flow deposited beyond the drainage outlet and formed a deposition fan of 20,400 m^3, with the largest depth over 2 m. The material composition of both the source and deposit materials was obtained through soil tests

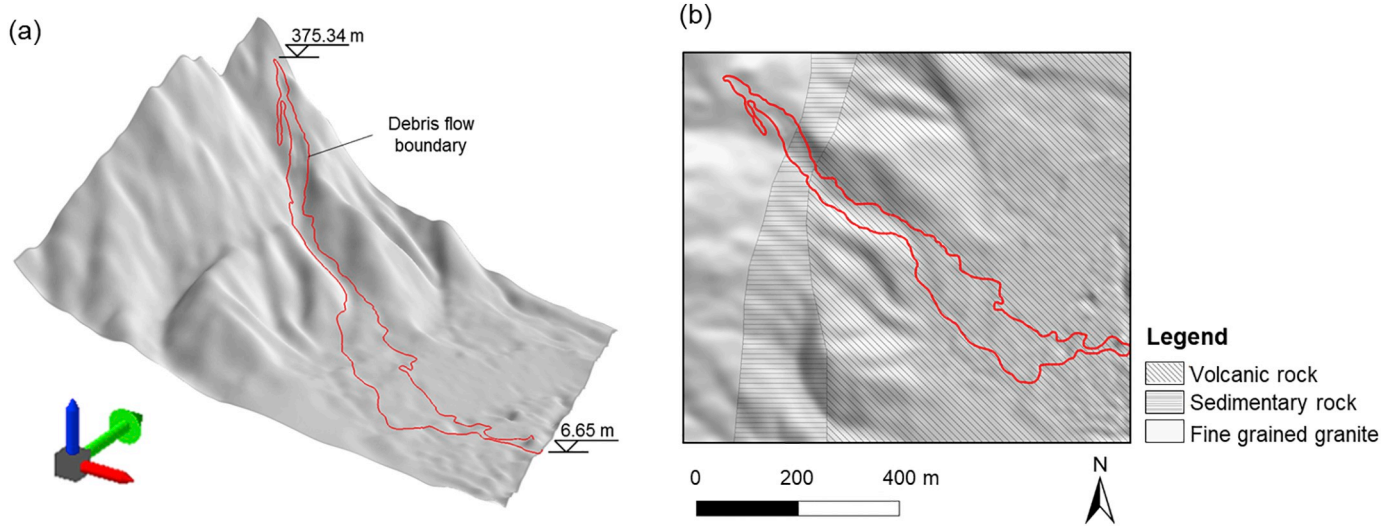

Fig. 2. Digital elevation model (a) and surface lithology (b) of the study area. The debris flow covered area is marked with a red line. More details of cross sections and lithology are available at GEO's website: https://www.cedd.gov.hk/eng/publications/geo/geo-reports/geo_rpt281/index.html. (For interpretation of the references to colour in this figure legend, the reader is referred to the web version of this article.)

and field investigations. The source materials were mainly granite colluvium (slope deposits) and, to a lesser extent, weathered bed rocks (granite, sedimentary rock and volcanic rock). The materials eroded and entrained along the steep drainage line were bouldery colluvium. The deposit mass was mainly poorly sorted clasts up to boulder size, supported by a poorly sorted mixture comprising granite boulders (up to 5 m diameter) and cobbles with sand and gravel as well as silt and clay. Vegetation, broken concrete, pipes and general garbage were also present in the deposit.

More detailed study indicates that the "parent" landslide was most relevant to the large debris flow for several reasons: (1) it was located at a high elevation of 300 mPD; (2) its volume was more than 2000 m^3, which to some extent was responsible for the final debris flow volume; (3) the presence of sufficient fine contents in the landslide reduced the soil permeability to form slurry flow; (4) its loose state caused contractive shearing behaviour and positive pore pressure build-up, reducing the flow resistance and inducing a rapid failure process; (5) its location in a drainage line led to concentration of the surface and subsurface flow.

3. Data and methods

3.1. Data

A digital terrain model (DEM) used in this study was generated after the 1990 debris flow event by GEO with a spatial resolution of 5 m. The two landslides were also depicted in the DEM. Detailed entrainment and deposition volumes within each sub-segment along the chainage can be found in the GEO Report No. 281 (King, 2013), as well as other properties for source materials and deposits such as grain size distribution. The post-event cross sections along the chainage with field checking are also available. The rainfall process from 10 Sept. to 11 Sept. 1990 associated with the debris flow was recorded at 15 minute-interval at rain gauge N07 installed by Hong Kong Observatory that was the closest rain gauge to the debris flow catchment. This rain gauge was located in the Tuen Mun Valley, less than 1.5 km from the catchment. The readings at gauge N07 may reasonably be considered the maximum that was likely to have fallen at the site. The hourly rainfall data from N07 is presented in Fig. 3.

3.2. Simulation framework

An integrated numerical program EDDA 2.0 (Shen et al., 2018) is used to simulate the initiation and dynamics of debris flows. The flowing mass is considered as a continuous flow. The governing equations, including the mass conservation and momentum equations, are in a depth-integrated form and solved in two dimensions using a finite difference scheme. The physical processes of rainfall infiltration, entrainment, and deposition of debris can be included. Infiltration is calculated by comparing the rainfall intensity with the saturated permeability of the surface soil; runoff will be generated if the rainfall intensity is larger than the saturated permeability. Three entrainment models are adopted in the program, which will be introduced in the next section. A digital elevation model is used to discretize the study area into a grid system. Every cell in the grid system carries topographic, geological, geotechnical and hydrological information for numerical simulation. The final runout distance, inundation area, deposition volume and entrainment magnitude of the debris flow can be compared with the field observations. Details of the program and its numerical scheme have been presented in Chen and Zhang (2015) and Shen et al. (2018).

3.3. Entrainment models

Material entrainment is a very complex and rapid process. Some of the mechanisms underlying entrainment in debris flow are summarised by Hungr et al. (2005) such as bed destabilization, erosion and bank collapse. In this study, three entrainment rate models, including one quasi-mechanical and two empirical models, are compared (Fig. 4): (1) the erosion model proposed by Iverson and Ouyang (2015) (referred to "Iverson-Ouyang model", Fig. 4a); (2) the linear erosion model with the erosion resistance coefficients determined by field erosion tests (e.g. Graf, 1984; Hanson and Simon, 2001; Julian and Torres, 2006; Chang et al., 2011) (referred to "Linear-Ex model", Fig. 4b); and (3) the linear erosion model with the bed erosion described as a Mohr-Coulomb failure process (e.g. Medina et al., 2008; Quan Luna et al., 2012) (referred to "Linear-MC model", Fig. 4c).

The Iverson-Ouyang entrainment model satisfies a boundary momentum jump condition, assuming a constant density of the flowing mixture and ignoring the effects from topography:

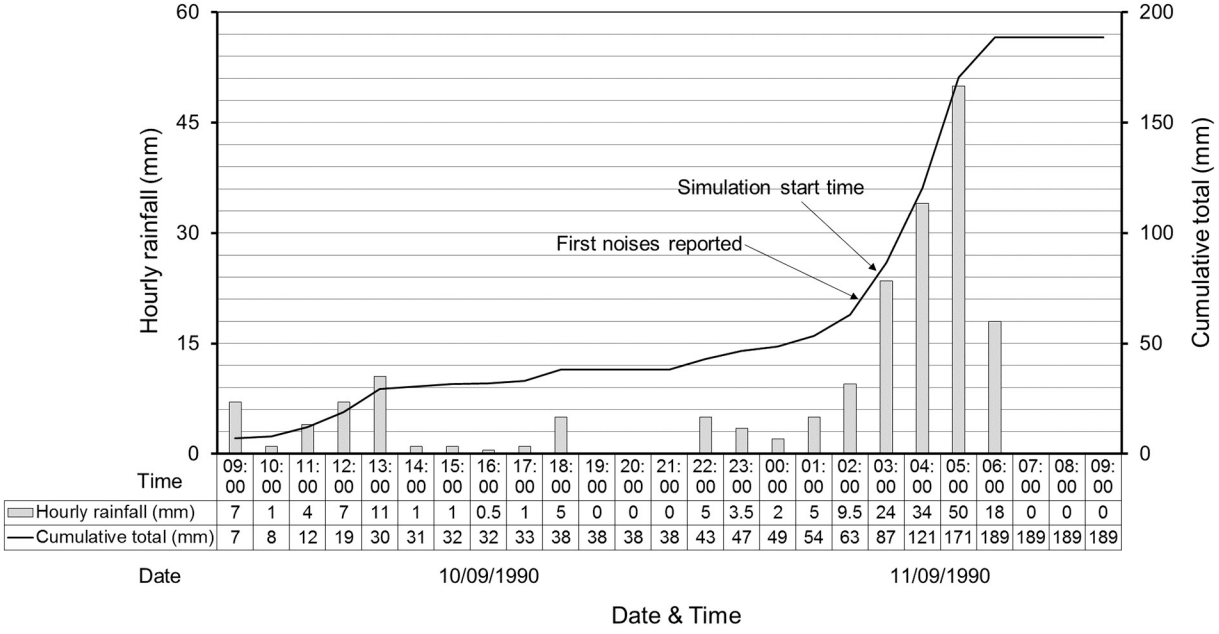

Time	09:00	10:00	11:00	12:00	13:00	14:00	15:00	16:00	17:00	18:00	19:00	20:00	21:00	22:00	23:00	00:00	01:00	02:00	03:00	04:00	05:00	06:00	07:00	08:00	09:00
Hourly rainfall (mm)	7	1	4	7	11	1	1	0.5	1	5	0	0	0	5	3.5	2	5	9.5	24	34	50	18	0	0	0
Cumulative total (mm)	7	8	12	19	30	31	32	32	33	38	38	38	38	43	47	49	54	63	87	121	171	189	189	189	189

Fig. 3. Rainfall data from rain gauge No. N07 from 10 Sept. to 11 Sept. 1990 (adapted from King, 2013).

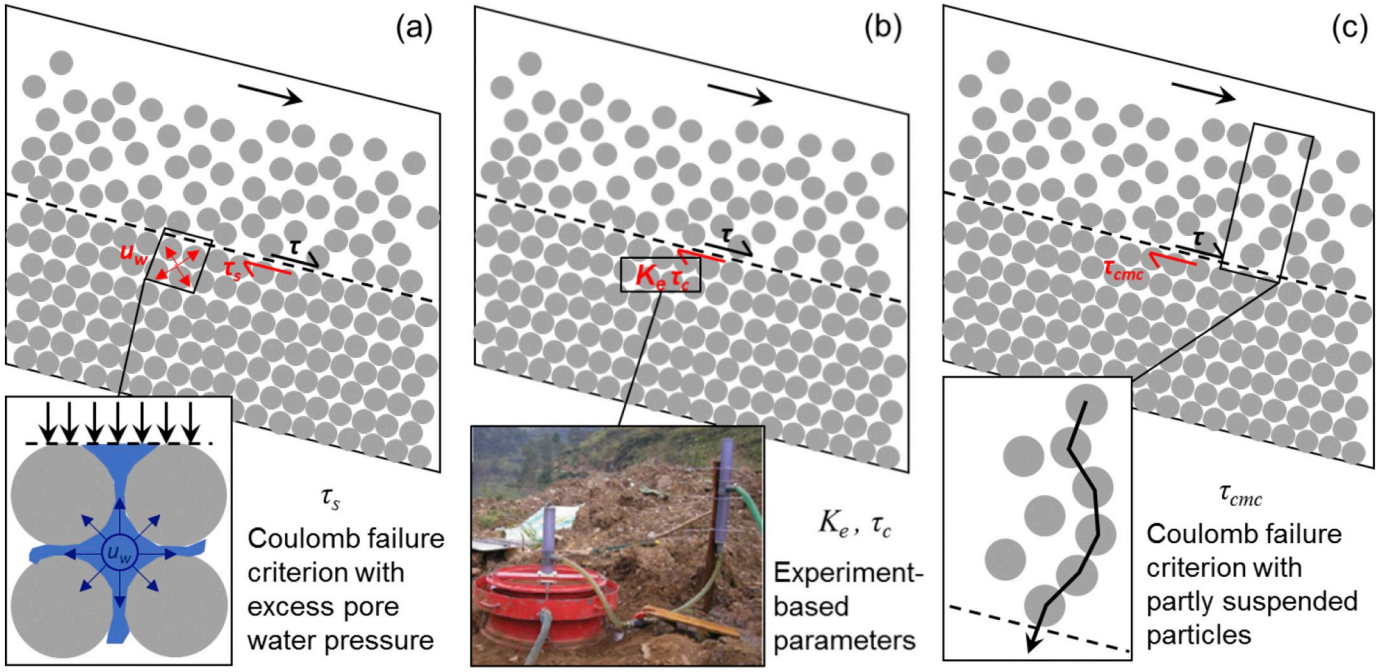

Fig. 4. Physical meaning of three entrainment models: (a) Iverson-Ouyang model: the entrainment rate formula must satisfy a boundary momentum jump condition; the density of the flowing mixture is assumed to be constant and the effects from topography are neglected; the critical erosive shear stress τ_s is assumed to obey the Coulomb failure criterion considering the degree of liquefaction of the bed material caused by the passing debris flow. (b) Linear-Ex model: the erosion rate is described by the commonly used linear empirical equation; the critical erosive stress τ_c and the coefficient of erodibility K_e are directly determined from field tests. (c) Linear-MC model: the erosion rate is also described by the linear equation with the critical erosive stress τ_{mc} assumed to obey the Coulomb failure criterion considering the effects of suspended particles in the debris flow mixture.

$$i = -\frac{\partial z_b}{\partial t} = \frac{\tau - \tau_s}{\rho V} \tag{1}$$

where z_b is the elevation (m) of erodible bed layer; t is time (s); ρ is the density of debris flow mixture; V is the depth-averaged debris flow velocity; τ is the total basal shear stress acting on the erodible surface from the flow layer and τ_s is the total shear resistance of the erodible layer surface (Pa). The basal resistance shear stress τ_s is assumed to follow the Coulomb failure criterion considering the degree of liquefaction of the bed material caused by the overriding debris flow (Fig. 4a):

$$\tau_s = c + (1 - \lambda)\rho g h \cos^2\beta \tan\phi_{bed} \tag{2}$$

where c and ϕ_{bed} are the cohesion (Pa) and friction angle (°) of the erodible bed material; g is the gravitational acceleration; β is the bed slope; $\cos^2\beta$ here accounts for the effective normal stress on the inclined channel bed assuming a hydrostatic pressure distribution within the debris flow; ρ is the density of debris flow mixture; λ is an empirical pore pressure ratio that numerically reflects the degree of liquefaction of the erodible bed, obtained from trial and error tests. In a debris flow event, the degree of liquefaction evolves dynamically as the fluid fraction evolves (Pudasaini, 2012; Pudasaini and Krautblatter, 2014). Parameter λ ranges from 0 (totally dry bed) to 1 (completely saturated soil). Numerical tests suggest that values of λ ranging from 0.5 to 0.8 give predictions of entrainment rates consistent with measurements in large-scale debris-flow experiments in which wet sediment beds liquefied almost completely (Iverson, 2012). It is necessary to mention that Eq. (1) produces singularity as the flow velocity becomes very small. Similarly, as the solid volume fraction evolves during the flow and entrainment process, the mixture density evolves dynamically. These shortcomings have been removed by Pudasaini and Fischer (2016) by presenting a mechanical two-phase entrainment model (Ren et al., 2018; Wang et al., 2018; Yang et al., 2018; Li et al., 2019). In the present study, Eq. (2) is used for simplicity. A certain threshold velocity, $v_{threshold}$, is set to avoid impossible large entrainment rate at very small V values (e.g. Lê and Pitman, 2009; Ouyang et al., 2015).

Other two erosion models, called Linear-Ex and Linear-MC, are of empirical nature with several parameters. In the Linear-Ex model, the erosion rate can be described by the commonly used linear empirical equation where the critical erosive stress τ_c and the coefficient of erodibility K_e are directly determined from experiments (Fig. 4b):

$$i = -\frac{\partial z_b}{\partial t} = K_e(\tau - \tau_c) \tag{3}$$

where τ is the total basal shear stress acting on the erodible surface from the flow layer (Pa); K_e is the coefficient of erodibility (m^3/N-s); τ_c is the critical erosive shear stress at the initiation of bed erosion (Pa). The latter two parameters describe the erosion resistance of the bed soil and can be measured in-situ using a jet index method (e.g. Chang et al., 2011; Zhu and Zhang, 2016).

In the Linear-MC model, the bed erosion is considered as a Mohr-Coulomb failure process. Similar to the Linear-Ex model, the erosion rate is also described by a linear equation:

$$i = -\frac{\partial z_b}{\partial t} = K_{mc}(\tau - \tau_{mc}) \tag{3}$$

where K_{mc} is a back-analysed parameter and the critical erosive shear stress τ_{mc} is calculated by considering limit equilibrium of partly suspended particles using the Mohr-Coulomb equation (Fig. 4c):

$$\tau_{mc} = c + (1 - C_s)C_v(\rho_s - \rho_w)gh\cos^2\beta \tan\phi_{bed} \tag{4}$$

where c and ϕ_{bed} are the cohesion (Pa) and friction angle (°) of the erodible bed material, respectively; β is the bed slope; C_s is the coefficient of suspension of solid particles and (1 - C_s) represents the portion of solid particles that are in contact; ρ_s is the density of solid particles; ρ_w is the density of water.

The shear stress, τ, can be computed as follows:

$$\tau = \rho g h S_f \tag{5}$$

where ρ is the density of debris flow mixture and S_f is the energy

Table 2
Rheological and computational parameters for debris flow.

Manning's coefficient	Laminar flow resistance	$\tau_y = \alpha_1 e^{\beta_1 C_v}$		$\mu = \alpha_2 e^{\beta_2 C_v}$		Deposition coefficient	Coefficient of suspension of solid particles
n	K	α_1	β_1	α_2	α_2	δ_d	C_s
0.16	2500	1.27×10^{-3}	22.8	2.97×10^{-4}	18.8	0.2	0.4

resistance slope.

Entrainment occurs when the volumetric sediment concentration of the debris flow, C_v, is smaller than an equilibrium value, $C_{v\infty}$. Here, C_v is defined as the ratio of the volume of solid materials to the volume of water and solid materials. The equilibrium volumetric sediment concentration $C_{v\infty}$ proposed by Takahashi et al. (1992) is adopted in this study:

$$C_{v\infty} = \frac{\rho_w \tan\beta}{(\rho_s - \rho_w)(\tan\varphi_{bed} - \tan\beta)} \tag{6}$$

where ρ_s is the density of soil particles (kg/m^3); ρ_w is the density of water (kg/m^3); and β is the bed slope.

3.4. Rheological model

The fluid flow is described using a suitable rheological model. Some rheological models are frequently used, such as the Coulomb viscous model (Laigle and Coussot, 1997), the Voellmy friction model (Medina et al., 2008), and the quadratic model (O'Brien et al., 1993). In the program, the quadratic rheology is used to consider the combined effects of different resistance terms. The resistance slope, S_f, is the sum of the yield slope, the viscous slope and the turbulent dispersive slope. The quadratic rheology expresses S_f as

$$S_f = \frac{\tau_y}{\rho g h} + \frac{K\mu V}{8\rho g h^2} + \frac{n_{td}^2 V^2}{h^{4/3}} \tag{7}$$

where h and V are the flow depth (m) and depth-integrated velocity (m/s), respectively; ρ is the mass density (kg/m^3) of the debris flow mixture; τ_y and μ are the yield stress (Pa) and dynamic viscosity (Pa·s) of the debris flow mixture, respectively; K is a laminar flow resistance coefficient; n_{td} is an equivalent Manning's coefficient accounting for both the turbulent behaviour and the resistance arising from solid-particle contacts. The following empirical relationships by O'Brien and Julien (1988) are adopted to estimate τ_y and μ:

$$\tau_y = \alpha_1 e^{\beta_1 C_v} \tag{8}$$

$$\mu = \alpha_2 e^{\beta_2 C_v} \tag{9}$$

where α_i and β_i are empirical coefficients determined by laboratory experiments. The equivalent Manning coefficient n_{td} is expressed as (FLO-2D Software Inc., 2009):

$$n_{td} = 0.0538 n e^{6.0896 C_v} \tag{10}$$

where n is the Manning coefficient.

3.5. Material deposition

The solid materials of a debris flow start to deposit when the flow velocity is smaller than a critical value and the volumetric sediment concentration C_v is larger than the equilibrium value, $C_{v\infty}$. The critical flow velocity proposed by Takahashi et al. (1992) is:

$$V_e = \frac{2}{5 d_{50}} \left(\frac{g \sin\theta_e \rho}{0.02 \rho_s} \right)^{0.5} \lambda^{-1} h^{1.5} \tag{11}$$

where

$$\tan\theta_e = \frac{C_v(\rho_s - \rho_w)\tan\varphi_{bed}}{C_v(\rho_s - \rho_w) + \rho_w} \tag{12}$$

$$\lambda^{-1} = \left(\frac{C_{v*}}{C_v} \right)^{1/3} - 1 \tag{13}$$

$$\rho = C_v(\rho_s - \rho_w) + \rho_w \tag{14}$$

in which d_{50} is the mean particle size of the debris flow material, which is assumed to be the same as that of the landslide deposit since the deposit soil is the source material of the debris flow. The rate of deposition can be expressed as

$$i = \delta_d \left(1 - \frac{V}{p V_e} \right) \frac{C_{v\infty} - C_v}{C_{v*}} V \tag{15}$$

where δ_d is a coefficient of deposition rate; p (< 1) is a dimensionless coefficient accounting for the location difference, and a value of 0.67 is recommended (Takahashi et al., 1992); C_{v_*} is the volume fraction of solids in the erodible bed. It should be noted that, in the deposition model, some coefficients such as deposition rate δ_d and location parameter p were determined empirically, which would be better automatically determined by the model during the interactive flow and deposition process between the applied shear stress by the flow and the resistance from the basal surface (Pudasaini and Fischer, 2016).

3.6. Model parameters

In this study all the bed soil properties are assumed to be uniform over the entire study area without considering spatial uncertainties. The parameters are summarised in Tables 2–4. The superficial erodible soil is the first to be physically defined. Geotechnical Control Office (GCO) conducted a series of comprehensive experiments and field investigations on the geology, hydrology and surficial soil properties all over Hong Kong. According to Geotechnical Control Office (1982), test results for shear strength are scattered. We select a least square regression line to determine cohesion c and friction angle ϕ_{bed}, which are set as 5.0 kPa and 42°, respectively. A typical value of saturated permeability of 1.0×10^6 (m/s) is selected. The density of solid material, ρ_s, is given as 2650 kg/m^3. The thickness of erodible bed is correlated to the slope angle, and an empirical relation established by Gao et al. (2016) is used to generate an erodible bed thickness map.

Table 3
Soil properties.

Mean grain size (mm)	Solid particle density (kg/m^3)	Saturated permeability (m/s)	Volume fraction of solids in erodible bed	Friction angle of erodible bed (°)	Cohesion of erodible bed (kPa)
d_{50}	ρ_s	k_s	C_{v_*}	ϕ_{bed}	c
20	2650	1.0×10^6	0.5	42.0	5.0

Table 4
Parameters for three entrainment models.

Iverson-Ouyang		Linear-Ex		Linear-MC
Threshold velocity (m/s)	Pore pressure ratio	Coefficient of erodibility (mm^3/N-s)	Critical erosive shear stress (Pa)	Erodibility coefficient (mm^3/N-s)
$V_{threshold}$	λ	K_e	τ_c	K_{mc}
3.0	0.55	50	5.0	250

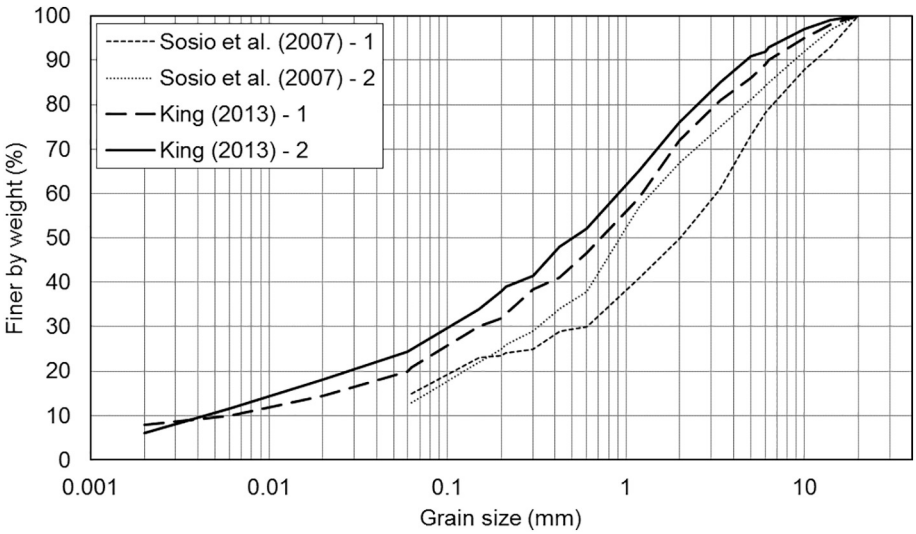

Fig. 5. Comparison of grain size distributions of two samples of the debris flow deposits in Sosio et al. (2007) and the envelopes for the Tsing Shan debris flow deposit in King (2013). Sample particle diameter < 20 mm.

Other parameters such as d_{50} and rheological parameters α_i and β_i are closely related to the particle size distribution. Based on the particle size distributions of the Tsing Shan debris samples (King, 2013), the clay to silt content ranges from 10 to 20% of the fraction finer than 20 mm. Sosio et al. (2007) conducted similar investigations on a debris flow in Central Italian Alps. The clay to silt content ranges from 5 to 15% of the fraction finer than 20 mm. As shown in Fig. 5, the particle size distribution curves for two events are similar. Despite the difference in the geological conditions of the two study areas, the rheology parameters determined for that event can be adopted in this study considering the similarity in the particle size composition. Therefore, α_1 and β_1 for τ_y are taken as 1.27×10^{-3} and 22.8, respectively; α_2 and β_2 for μ are taken as 2.97×10^{-4} and 18.8, respectively (Sosio et al., 2007). As mentioned previously, the vegetation cover in the study area is not dense and the ground cover can be classified as sparse vegetation following FLO-2D Software Inc. (2009), leading to a value of K as 2500. The Manning's coefficient is set to be 0.16. Through back analysis, the volume fraction of solids in the erodible bed, C_{v_s}, is set to be 0.5.

4. Simulation results

The simulation started from 1 h before the mobilization of the two landslides, i.e. 2:00 am on 11 September 1990. The corresponding rainfall process is shown in Fig. 3. After 1 h of simulation, the mass of the “Trigger” and “Parent” landslides is released at the location of the “Parent” landslide (Fig. 1). The landslide mass is treated as a fluid with the given rheological properties. Possible transformation from landslide to debris flow is not considered.

The final distribution of erosion and deposition depths at the end of simulation are shown in Fig. 6. For the Iverson-Ouyang model (Fig. 6a), the simulated eroded area is located between Ch 100 and Ch 500, which is the upper entrainment area. The simulated erosion area mostly lies within the observed debris flow track. The final distribution of the debris flow deposition is also presented (Fig. 6b). Most deposition is simulated to occur after Ch 500, which corresponds well to the judgment from the field investigations that the main deposition area is located downstream Ch 500. The runout distance is slightly shorter than the observed value. Some deposition zone falls outside the observed range, but most of the deposition area matches well with the observed range.

The simulation results from the three entrainment models and the debris flow records are summarised in Table 5. Generally, all of the three models perform acceptably well. The erosion and deposition volumes simulated by the Iverson-Ouyang and Linear-MC models are slightly less than the observed values, while the Linear-Ex model slightly overestimates the volumes. The maximum erosion and deposition depths simulated by the models are close to the records. The maximum flow velocity is estimated empirically to be 16.5 m/s at Ch 350 and 12.5 m/s at Ch 475.

For the Linear-Ex entrainment model, the final erosion distribution is shown in Fig. 6c. The most eroded area is simulated to be located between Ch 100 and Ch 500, but is more widespread compared with the Iverson-Ouyang model result. The simulated erosion area generally falls on the observed debris flow track. The final distribution of the debris flow deposition depth is presented in Fig. 6d. The simulation result corresponds well to the field observation: the downstream area after Ch 500 is the main deposition area. The runout distance is also very close to the observed value. Only a small part of the deposition zone falls outside the observed range.

Using the Linear-MC entrainment model, the calculated final erosion distribution is shown in Fig. 6e. The most eroded area is located between Ch 100 and Ch 300 that is most concentrated among the three cases. The simulated debris flow area generally falls within the observed debris flow track. As presented in Fig. 6f, the final distribution of the debris flow deposition zone is very similar to that from the Linear-Ex model. Most of the simulated erosion and deposition was inside the

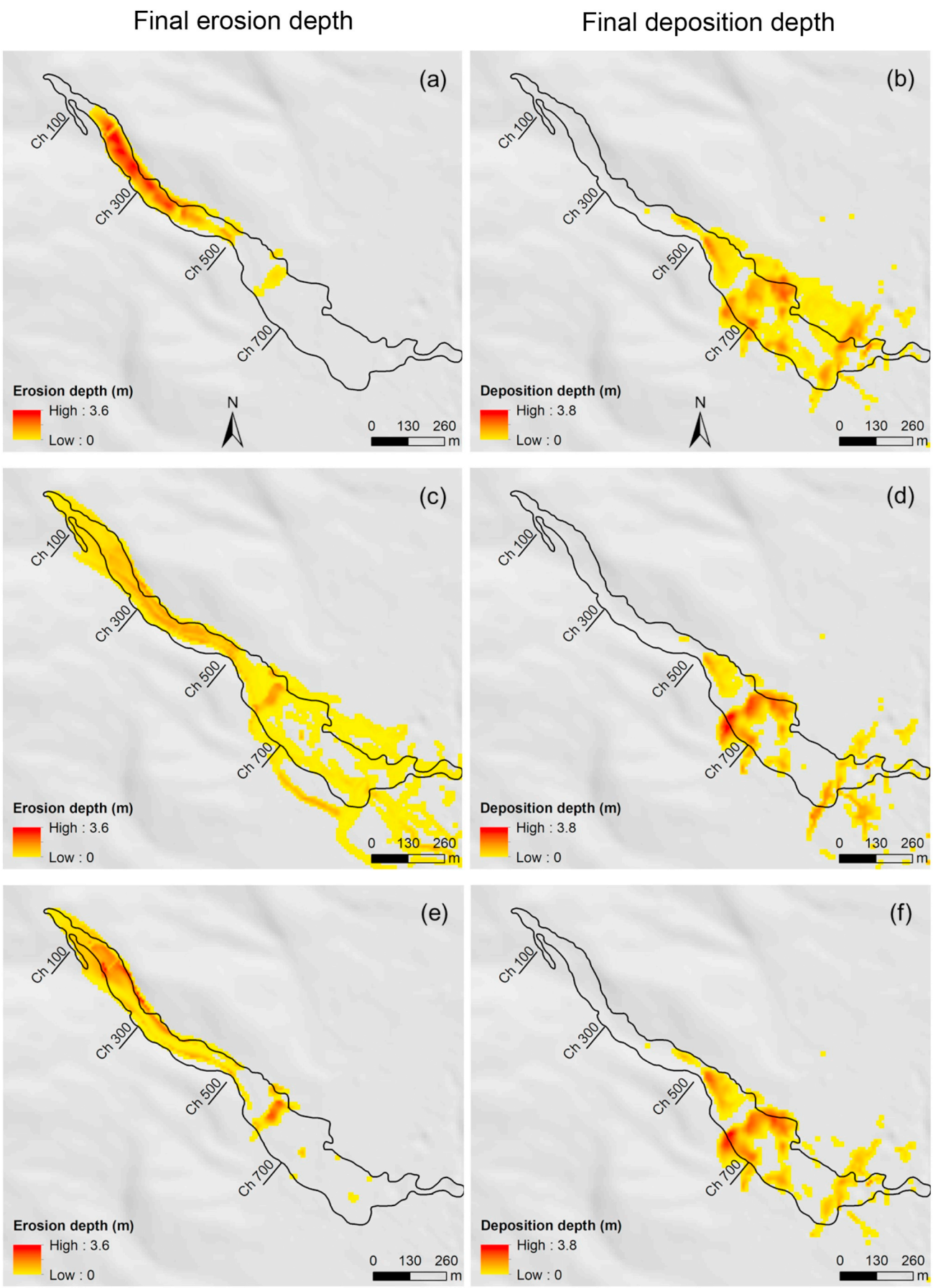

Fig. 6. Distributions of final erosion depth and deposition depth at the end of simulation: (a) and (b) Iverson-Ouyang model; (c) and (d) Linear-Ex model; (e) and (f) Linear-MC model.

Table 5
Summary of real debris flow data and simulation results.

Results	Observed value	Iverson-Ouyang	Linear-Ex	Linear-MC
Erosion volume (m^3)	14,630	16,019	21,000	11,200
Deposition volume (m^3)	20,400	18,900	25,800	18,000
Max erosion depth (m)	~3	3.4	2.0	3.6
Max deposition depth (m)	~3	2.6	3.6	3.8
Max velocity (m/s)	12.5–16.5	12.0	11.0	9.0

debris flow covered area. However, a small part of the simulated erosion and deposition zone is outside the flow covered area. This may be because the elevation model was obtained after the debris flow event and the spatial uncertainties in the model parameters were not considered.

A comparison between the simulated and observed entrainment and deposition volumes along the debris flow track is shown in Fig. 7a and b, respectively. The field observation illustrates that erosion is somewhat uniformly distributed along the flow path. In the Iverson-Ouyang model case, erosion is concentrated before Ch 500. While in both the linear models, erosion is more scattered. By comparing the observed and simulated deposition distributions along the track, it can be concluded that all of the three simulations give acceptable results, with significant deposition occurring between Ch 500 to Ch 835.

Fig. 8 presents the discharge process and the evolution of volumetric sediment concentration, *Cv,* at Ch 500. The timeline starts after the initiation of debris flow (1 h/3600 s). In the Iverson-Ouyang model, the debris flow lasts for about 40 s, with a peak discharge of about 1800 m^3/s. In the Linear-Ex and Linear-MC models, the discharge process is longer and the peak discharge is around 190 m^3/s, which is more realistic than that from the Iverson-Ouyang model. When the debris flow front reaches Ch 500, C_v increases very quickly to a peak value of about 0.5. In the Iverson-Ouyang model, C_v drops more quickly than that in the Linear models, as a result of very fast marching of the debris flow. For the two Linear models, C_v decreases gradually to a lower level, which can be viewed as a hyper-concentrated flow induced by further erosion behind the debris flow front. In the Linear-Ex model,

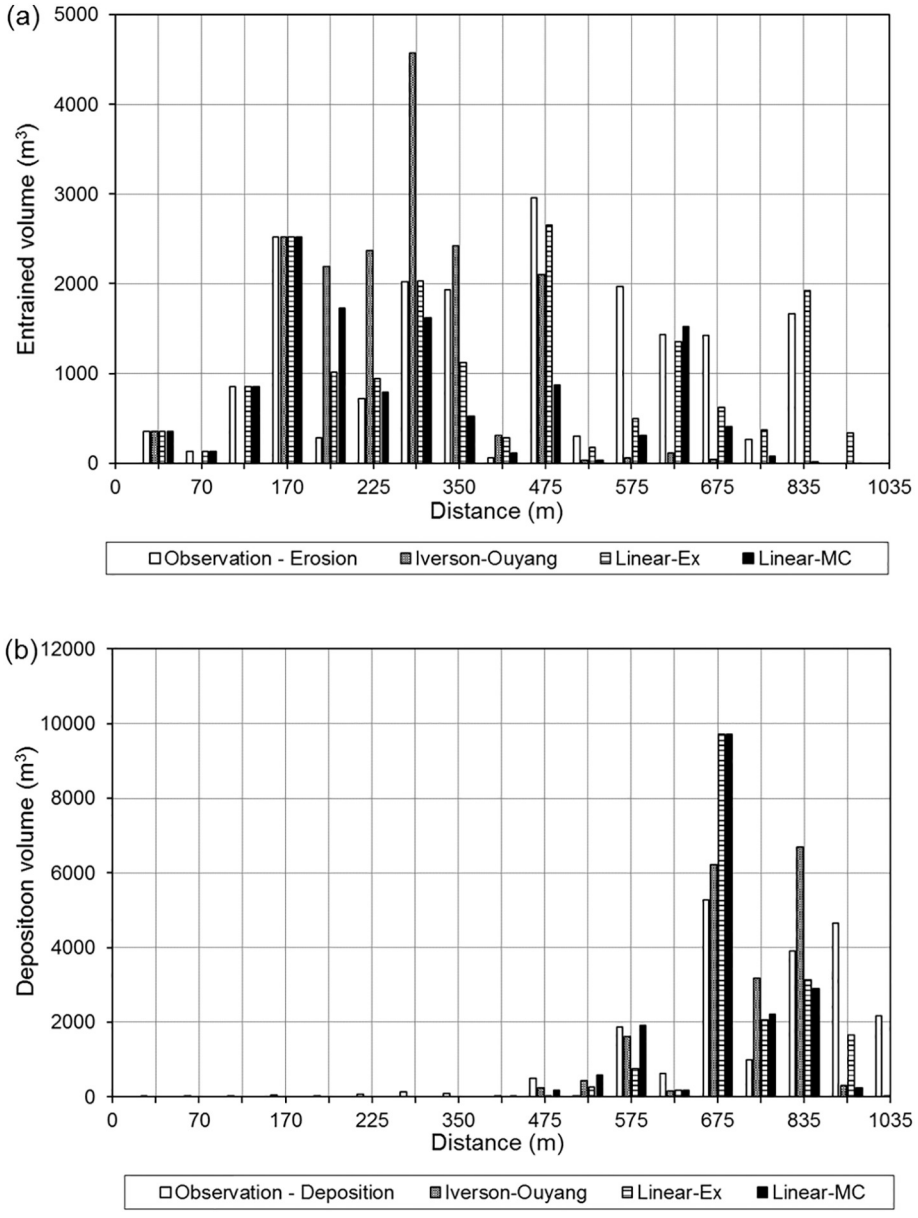

Fig. 7. Variation of (a) material entrainment and (b) deposition volume along the flow distance.

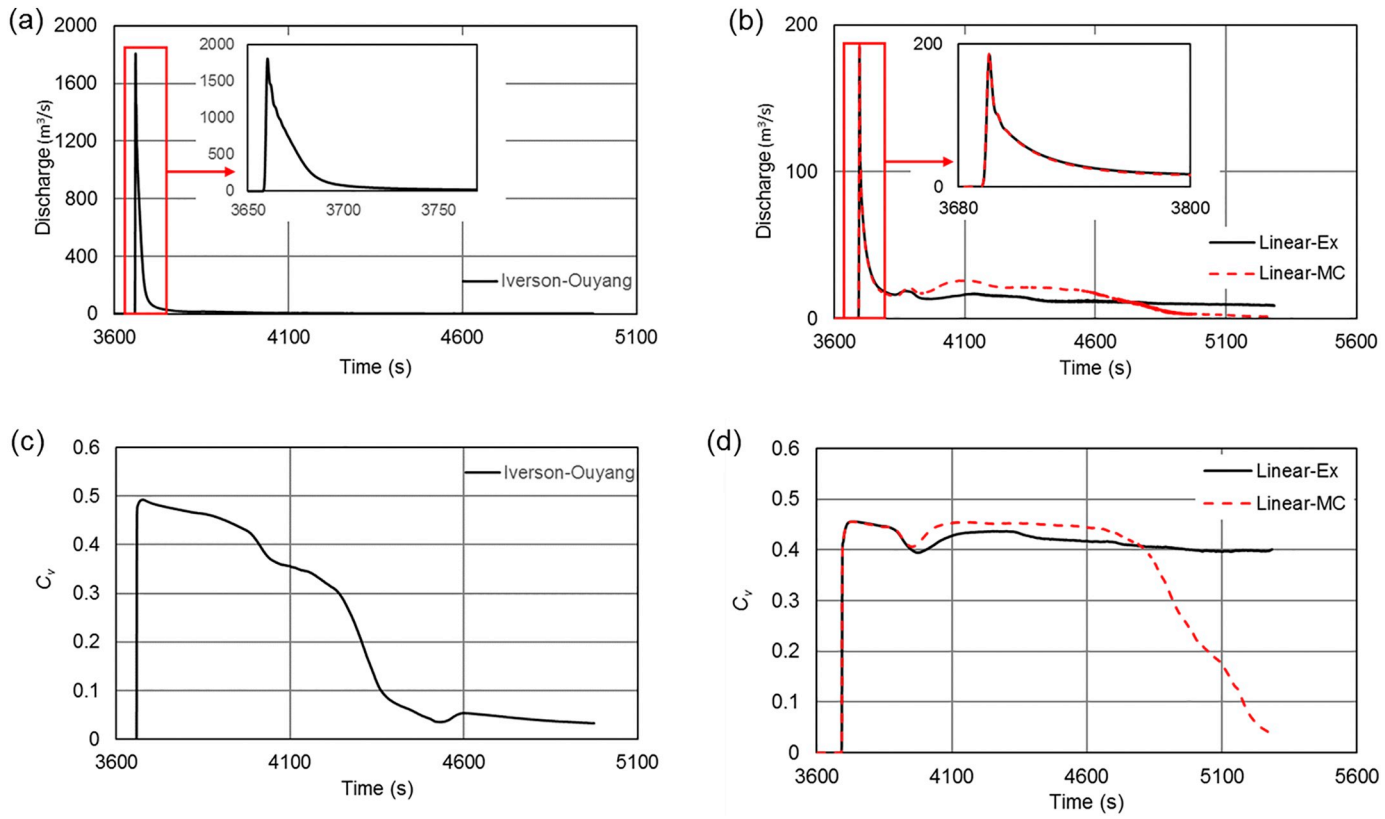

Fig. 8. The discharge hydrograph of debris flow and changes in volumetric solid concentration (C_v) at Ch500 after the debris flow was initiated at t = 3600 s: Iverson-Ouyang model with (a) discharge process and (b) sediment concentration changes; Linear-Ex and Linear-MC model with (c) discharge process and (d) sediment concentration changes.

high values of sediment concentration are maintained for a very long time; however, the Linear-MC model predicts a flowing process of only about half an hour.

5. Discussion

Entrainment is a very important mechanism in debris flow dynamics. Many entrainment models have been proposed to study this phenomenon. In this study, the Iverson-Ouyang model and the Linear-MC model give a relatively concentrated entrainment area in steep slope parts (Fig. 6a and e) where high debris flow velocity and discharge rate occur and induce large shear stresses on the bed surface. In flat areas downstream Ch 500, entrainment is not simulated by the two models. The critical shear stress in the two models is computed by the Mohr-Coulomb failure criterion with a magnitude of kPa. Entrainment occurs only when the shear stress acting on the bed soil by the debris flow mass exceeds the shear resistance of the bed soil. In flat areas the velocity and discharge of the debris flow are much smaller than those in the steep slopes. Thus no entrainment is simulated by the two models. For the Linear-Ex model, the critical shear stress is obtained from field experiments (e.g. a jet index method). The resulting value of the critical shear stress is of magnitudes of several to dozens Pa (Zhu and Zhang, 2016; Shen et al., 2017). The threshold of entrainment occurrence is much lower than that in the two other models, which results in an extensive entrainment area covering both the upper steep part and the lower deposition part (Fig. 6c).

The Iverson-Ouyang model produces a much larger but ephemeral entrainment rate. Erosion occurs very fast and intensively. A large volume of solid materials enters the flowing mixture, resulting in a high discharge rate compared with the other models (Fig. 8a). The resulting higher mobility is closely associated with the larger entrainment rate in the mass flow. This has been shown with a mechanical erosion model for two-phase particle fluid mixture debris flows by Pudasaini and Fischer (2016). They proved that reduced friction in erosion is equivalent to momentum production and erosion enhances the mass flow mobility. Furthermore, they stated that “As the mass is added into the system, the gravity load immediately accelerates the total mass down the entire travel distance. This further enhances the flow mobility, because the erosion-induced added mass implies added potential energy.” The resulting debris flow surge marches rapidly, followed by a clear water flow that does not induce entrainment due to the large critical shear stress (Fig. 8c).

On the other hand, the Linear-Ex model produces a mild but prolonged entrainment process. The final erosion depth is smaller than that in the Iverson-Ouyang model; however, the eroded area covers the whole debris flow track including the deposit area (Figs. 6c and 7a). This is due to the empirical entrainment equation and parameters that give a low threshold for entrainment so that entrainment can occur even in the flat area. Moreover, as reported by King (2013), the flooding in the late part of the event was responsible for further gully erosion and redistribution of the earlier flow deposits. The entrainment in the late stage of the rainstorm is simulated by the Linear-Ex model. Hyperconcentrated flow with solid concentration is generated following the main debris flow surge (Fig. 8d) with a certain solid concentration for a long period. This can also be explained by the low critical shear stress used in the Liner-Ex model. The low threshold given by the model allows entrainment by runoff water that continues to move bed solid mass after the debris flow surge.

The Linear-MC model produces results somewhere between the above two models. The entrainment equation is empirical but the Mohr-Coulomb criterion is adopted to compute the critical shear stress. By comparing the simulated entrainment patterns with the field observations, it is found that the Linear-Ex model simulated entrainment for both the debris flow surge and the posterior rainfall runoff (Fig. 8d). In

general, all three models simulate the entrainment volume reasonably well; however, instead of using a single-phase rheological model with empirical parameters obtained from experiments, more mechanically-based models might be further adopted for entrainment simulation (Pudasaini and Fischer, 2016). The presented results (Table 5) with respect to the three entrainment models substantially depend on some parameter values that need to be calibrated by trial and error without rigorous physical constrains, such as K_{mc}, λ, and $v_{threshold}$. The simulation results are especially sensitive to λ and $v_{threshold}$ in the Iverson-Ouyang model, K_{mc} and C_s in the Linear-MC model, and K_e and τ_c in the Linear-Ex model. One cannot easily justify which model is better over the other. Similarly, since the debris flow material is usually composed of solid particles and viscous fluid, better and more reliable results could be obtained by using two-phase, or even multi-phase mass flow models (e.g. Pudasaini, 2012; Li et al., 2018; Pudasaini and Mergili, 2019) and mechanical two-phase entrainment models (Pudasaini and Fischer, 2016). Moreover, spatial variations and uncertainties in the geotechnical, geomorphological and hydrogeological parameters (e.g. Xiao et al., 2017; Fenton et al., 2018; Zhang et al., 2018), and the mechanical and hydrological vegetation-soil interactions (Zhu and Zhang, 2019) are not considered in this study. Spatial uncertainties might also be considered in the future.

6. Summary and conclusions

A debris-flow modelling program, EDDA 2.0, is used to evaluate the performance of three entrainment analysis models, including the Iverson-Ouyang model and two linear models with different concepts of erosion resistance using the well documented Tsing Shan debris flow that occurred in Hong Kong in September 1990 as a benchmark. Most of the simulation parameters can be determined from field and laboratory test results with minor adjustments based on field conditions.

All the three entrainment models perform reasonably well, giving satisfactory accuracy of the total entrainment magnitude, deposition volume, inundation area and runout distance compared with the field observations. In the Iverson-Ouyang model, the entrainment area is concentrated in the upper part of the track with steep slope angles. The runout distance is slightly shorter than the observed value. The discharge duration given by this model is very short while the flow rate very large. The Linear-Ex entrainment model provides satisfactory performance in predicting the entrainment, deposition and discharge processes, but predicts a much longer flow duration with high sediment concentrations. The Linear-MC entrainment model leads to simulation results similar to those from the Linear-Ex model, with a discharge process of about half an hour. The results serve as a reference for selecting models for hazard analysis and risk assessment.

Declaration of Competing Interest

None.

Acknowledgements

The authors appreciate the Civil Engineering and Development Department of the HKSAR Government for offering access to the detailed documents of the Tsing Shan debris flow. The financial support from the Research Grants Council of Hong Kong (Grants Nos. 16206217 and UGC/FDS25/E11/17) is acknowledged.

References

FLO-2D Software Inc, 2009. FLO-2D User Manual, Version 2009. Nutrioso, Arizona.
van Asch, T.W.J., Tang, C., Alkema, D., Zhu, J., Zhou, W., 2014. An integrated model to assess critical rainfall thresholds for run-out distances of debris flows. Nat. Hazards 70 (1), 299–311.
Berti, M., Genevois, R., Simoni, A., Tecca, P.R., 1999. Field observations of a debris flow event in the Dolomites. Geomorphology 29 (3–4), 265–274.
Breien, H., De Blasio, F.V., Elverhøi, A., Høeg, K., 2008. Erosion and morphology of a debris flow caused by a glacial lake outburst flood, Western Norway. Landslides 5 (3), 271–280.
Chan, Y.C., Lam, C.H., Shum, W.L., 1991. The September 90 Tsing Shan Landslide: A Factual Report, Technical Note 4/91. Geotechnical Control Office, Hong Kong.
Chang, D.S., Zhang, L.M., Xu, Y., Huang, R.Q., 2011. Field testing of erodibility of two landslide dams triggered by the 12 May Wenchuan earthquake. Landslides 8 (3), 321–332.
Chen, H.X., Zhang, L.M., 2015. EDDA 1.0: integrated simulation of debris flow erosion, deposition and property changes. Geosci. Model Dev. 8, 829–844.
Chen, H.X., Zhang, L.M., Gao, L., Yuan, Q., Lu, T., Xiang, B., Zhuang, W.L., 2017. Simulation of interactions among multiple debris flows. Landslides 14 (2), 595–615.
Dai, Z.L., Huang, Y., Cheng, H.L., Xu, Q., 2014. 3D numerical modelling using smoothed particle hydrodynamics of flow-like landslide propagation triggered by the 2008 Wenchuan earthquake. Eng. Geol. 180, 21–33.
Fenton, G.A., Naghibi, F., Hicks, M.A., 2018. Effect of sampling plan and trend removal on residual uncertainty. Georisk 12 (4), 253–264.
Gao, L., Zhang, L.M., Chen, H.X., Shen, P., 2016. Simulating debris flow mobility in urban settings. Eng. Geol. 214, 67–78.
Geotechnical Control Office, 1982. Mid-Levels Study: Report on Geology, Hydrology and Soil Properties. Geotechnical Control Office, Hong Kong.
Graf, W.H., 1984. Hydraulics of Sediment Transport. Water Resources Publications, Colorado, pp. 513.
Hanson, G.J., Simon, A., 2001. Erodibility of cohesive streambeds in the loess area of the midwestern USA. Hydrol. Process. 15 (1), 23–38.
Hungr, O., McDougall, S., 2009. Two numerical models for landslide dynamic analysis. Comput. Geosci. 35 (5), 978–992.
Hungr, O., McDougall, S., Bovis, M., 2005. Entrainment of material by debris flows. In: Jakob, M., Hungr, O. (Eds.), Debris-Flow Hazards and Related Phenomena. Springer, Berlin, pp. 135–158.
Hutchinson, J.N., Bhandari, R.K., 1971. Undrained loading, a fundamental mechanism of mudflows and other mass movements. Géotechnique 21 (4), 353–358.
Iverson, R.M., 2012. Elementary theory of bed-sediment entrainment by debris flows and avalanches. J. Geophys. Res. 117 (F3).
Iverson, R.M., Ouyang, C.J., 2015. Entrainment of bed material by earth-surface mass flows: Review and reformulation of depth-integrated theory. Rev. Geophys. 53 (1), 27–58.
Iverson, R.M., Reid, M.E., Logan, M., LaHusen, R.G., Godt, J.W., Griswold, J.P., 2011. Positive feedback and momentum growth during debris-flow entrainment of wet bed sediment. Nat. Geosci. 4, 116–121.
Jakob, M., Anderson, D., Fuller, T., Hungr, O., Ayotte, D., 2000. An unusually large debris flow at Hummingbird Creek, Mara Lake, British Columbia. Can. Geotech. J. 37 (5), 1109–1125.
Johnson, A.M., Rodine, J.R., 1984. Debris flow. In: Brunsden, D., Prior, D.B. (Eds.), Slope Instability. John Wiley & Sons, Chichester, UK, pp. 257–361.
Julian, J.P., Torres, R., 2006. Hydraulic erosion of cohesive riverbanks. Geomorphology 76 (1–2), 193–206.
King, J.P., 2013. Tsing Shan Debris Flow and Debris Flood. Geotechnical Engineering Office, Civil Engineering and Development Department, Hong Kong. Online access. https://www.cedd.gov.hk/eng/publications/geo/geo-reports/geo_rpt281/index.html.
Kwan, J.S.H., Sun, H.W., 2007. Benchmarking exercise on landslide mobility modelling–runout analyses using 3dDMM. In: Ho, K., Li, V. (Eds.), Proceedings of the 2007 International Forum on Landslide Disaster Management. Geotechnical Engineering Office, Hong Kong, pp. 945–966.
Laigle, D., Coussot, P., 1997. Numerical modelling of mudflows. J. Hydraul. Eng. 123 (7), 617–623.
Lê, L., Pitman, E.B., 2009. A model for granular flows over an erodible surface. SIAM J. Appl. Math. 70 (5), 1407–1427.
Li, D.H., Xu, X.N., Huao, H.B., 2012. Formation conditions and the movement characteristics of “8.14” giant debris flow in Yingxiu Town, Wenchuan County, Sichuan Province. Chinese J. Geol. Hazard Control 23 (3), 32–38.
Li, J., Cao, Z.X., Hu, K.H., Pender, G., Liu, Q.Q., 2018. A depth-averaged two-phase model for debris flows over erodible beds. Earth Surf. Process. Landf. 43 (4), 817–839.
Li, P., Shen, W., Hou, X.K., Li, T.L., 2019. Numerical simulation of the propagation process of a rapid flow-like landslide considering bed entrainment: a case study. Eng. Geol. 263. https://doi.org/10.1016/j.enggeo.2019.105287.
McDougall, S., Hungr, O., 2005. Dynamic modelling of entrainment in rapid landslides. Can. Geotech. J. 42 (5), 1437–1448.
Medina, V., Hürlimann, M., Bateman, A., 2008. Application of FLATModel, a 2D finite volume code, to debris flows in the northeastern part of the Iberian Peninsula. Landslides 5 (1), 127–142.
Mergili, M., Jan-Thomas, F., Krenn, J., Pudasaini, S.P., 2017. r.avaflow v1, an advanced open-source computational framework for the propagation and interaction of two-phase mass flows. Geosci. Model Dev. 10 (2), 553–569.
Mergili, M., Emmer, A., Juřicová, A., Cochachin, A., Fischer, J.T., Huggel, C., Pudasaini, S.P., 2018a. How well can we simulate complex hydro-geomorphic process chains? The 2012 multi-lake outburst flood in the Santa Cruz Valley (Cordillera Blanca, Perú). Earth Surf. Process. Landf. 43 (7), 1373–1389.
Mergili, M., Frank, B., Fischer, J.T., Huggel, C., Pudasaini, S.P., 2018b. Computational experiments on the 1962 and 1970 landslide events at Huascarán (Peru) with r.avaflow: Lessons learned for predictive mass flow simulations. Geomorphology 322, 15–28.
O’Brien, J.S., Julien, P.Y., 1988. Laboratory analysis of mudflow properties. J. Hydraul. Eng. 114 (8), 877–887.

O'Brien, J.S., Julien, P.Y., Fullerton, W.T., 1993. Two-dimensional water flood and mudflow simulation. J. Hydraul. Eng. 119 (2), 244–261.
Ouyang, C.J., He, S.M., Tang, C., 2015. Numerical analysis of dynamics of debris flow over erodible beds in Wenchuan earthquake-induced area. Eng. Geol. 194, 62–72.
Pastor, M., Haddad, B., Sorbino, G., Cuomo, S., Drempetic, V., 2009. A depth-integrated, coupled SPH model for flow-like landslides and related phenomena. Int. J. Numer. Anal. Methods Geomech. 33 (2), 143–172.
Pudasaini, S.P., 2012. A general two-phase debris flow model. J Geophys. Res.-Earth 117 (F03010).
Pudasaini, S.P., Fischer, J.T., 2016. A mechanical erosion model for two-phase mass flows. arXiv:1610.01806.
Pudasaini, S.P., Krautblatter, M., 2014. A two-phase mechanical model for rock-ice avalanches. J Geophys. Res.-Earth 119 (10), 2272–2290.
Pudasaini, S.P., Mergili, M., 2019. A multi-phase mass flow model. J Geophys. Res.-Earth 124 (12), 2920–2942.
Quan Luna, B., Remaître, A., van Asch, T.W.J., Malet, J.P., van Westen, C.J., 2012. Analysis of debris flow behaviour with a one dimensional run-out model incorporating entrainment. Eng. Geol. 128, 63–75.
Ren, Z., Wang, K., Yang, K., Zhou, Z.H., Tang, Y.J., Tian, L., Xu, Z.M., 2018. The grain size distribution and composition of the Touzhai rock avalanche deposit in Yunnan, China. Eng. Geol. 234, 97–111.
Sassa, K., Wang, G.H., 2005. Mechanism of landslide-triggered debris flows: liquefaction phenomena due to the undrained loading of torrent deposits. In: Jakob, M., Hungr, O. (Eds.), Debris-Flow Hazards and Related Phenomena. Springer, Berlin, pp. 81–104.
Shen, P., Zhang, L.M., Chen, H.X., Gao, L., 2017. Role of vegetation restoration in mitigating hillslope erosion and debris flows. Eng. Geol. 216, 122–133.
Shen, P., Zhang, L.M., Chen, H.X., Fan, R.L., 2018. EDDA 2.0: integrated simulation of debris flow initiation and dynamics considering two initiation mechanisms. Geosci. Model Dev. 11, 2841–2856.
Sosio, R., Crosta, G.B., Frattini, P., 2007. Field observations, rheological testing and numerical modelling of a debris-flow event. Earth Surf. Process. Landf. 32 (2), 290–306.
Takahashi, T., Nakagawa, H., Harada, T., Yamashiki, Y., 1992. Routing debris flows with particle segregation. J. Hydraul. Eng. 118 (11), 1490–1507.
Wang, G., Sassa, K., Fukuoka, H., 2003. Downslope volume enlargement of a debris slide–debris flow in the 1999 Hiroshima, Japan, rainstorm. Eng. Geol. 69 (3–4), 309–330.
Wang, T., Chen, X.Q., Li, K., Chen, J.G., You, Y., 2018. Experimental study of viscous debris flow characteristics in drainage channel with oblique symmetrical sills. Eng. Geol. 233, 55–62.
Xiao, T., Li, D.Q., Cao, Z.J., Tang, X.S., 2017. Full probabilistic design of slopes in spatially variable soils using simplified reliability analysis method. Georisk 11 (1), 146–159.
Yang, H.Q., Xing, S.G., Wang, Q., Li, Z., 2018. Model test on the entrainment phenomenon and energy conversion mechanism of flow-like landslides. Eng. Geol. 239, 119–125.
Zhang, L.L., Wu, F., Zheng, Y.F., Chen, L.H., Zhang, J., Li, X., 2018. Probabilistic calibration of a coupled hydro-mechanical slope stability model with integration of multiple observations. Georisk 12 (3), 169–182.
Zhang, L.M., Xiao, T., He, J., Chen, C., 2019. Erosion-based analysis of breaching of Baige landslide dams on the Jinsha River, China, in 2018. Landslides 16, 1965–1979.
Zhou, S.Y., Gao, L., Zhang, L.M., 2019. Predicting debris-flow clusters under extreme rainstorms: a case study on Hong Kong Island. B. Eng. Geol. Env. 78, 5775–5794.
Zhu, H., Zhang, L.M., 2016. Field investigation of erosion resistance of common grass species for soil bioengineering in Hong Kong. Acta Geotech. 11 (5), 1047–1059.
Zhu, H., Zhang, L.M., 2019. Root-soil-water hydrological interaction and its impact on slope stability. Georisk 13 (4), 349–359.